Atom probe tomography characterization of solute segregation to dislocations and interfaces

M. K. Miller

Abstract The level and extent of solute segregation to individual dislocations and interfaces may be visualized and quantified by atom probe tomography. The large volume of analysis and high data acquisition rate of the local electrode atom probe (LEAP®) enables the solute distribution in the region of and along the core of dislocations to be estimated. Solute segregation at precipitate-matrix interfaces of precipitates as small as 2-nm diameter may be quantified. Examples are presented of solute segregation to dislocations and clustering/precipitation in a neutron irradiated Fe–Ni–P model alloy and the neutron irradiated beltline weld from the Midland reactor.

Introduction

Solute atom segregation to dislocations is one of the most difficult microstructure features to quantify due to the small extent of the segregation and the low dislocation densities in most materials. Typically, the extent of the solute segregation only extends a few nanometers in the vicinity of the stress field associated with the core of the dislocation. Therefore, microscopy techniques with high spatial resolution and single atom sensitivity for all elements are required to quantify the type and amount of segregation at dislocations. Atom probe tomography (APT) has the necessary spatial and mass resolutions to perform these types of analyses. These types of APT characterizations are generally best performed on cold worked or mechanically alloyed materials and irradiated materials where the dislocation density is significantly higher. In this paper, some examples of APT characterizations of solute segregation to dislocations and interfaces are presented.

Field ion microscopy

Some early attempts were made to characterize dislocations with field ion microscopy. Dislocations may be observed in field ion images by a change of the normal concentric atom terraces at crystallographic poles to spirals [1]. If a dislocation has a Burgers vector component normal to the plane of the specimen surface at its point of emergence on the hemispherical surface, the usual concentric rings in the field ion image will exhibit a spiral. However, if the point of emergence occurs in a high index region, the dislocation may not be evident in the field ion image. The visibility criterion for a perfect dislocation having a Burgers vector b and line vector l that converts a stack of planes of normal n into a spiral ramp is $n \cdot l \neq 0$ and $n \cdot b \neq 0$. Solute segregation may be directly evident in the field ion image by the presence of brightly imaging atoms near the point of emergence of the dislocation. However, this is only the case when the evaporation field for the segregant is significantly higher than that of the matrix. Some examples of this case are boron segregation to dislocations in Ni_3Al [2] and zirconium segregation

M. K. Miller (✉)
Microscopy, Microanalysis, Microscopy Group, Materials Science and Technology Division,
Oak Ridge National Laboratory, Building 4500S, MS 6136,
P.O. Box 2008, Oak Ridge, TN 37831-6136, USA
e-mail: millermk@ornl.gov

to dislocations in NiAl [3] and carbon in low-carbon martensite [4]. Similarly, solute segregation to grain and twin boundaries as well as other types of interfaces can also be detected by bright spot decoration [3, 5]. The nature of the segregation element cannot be conclusively confirmed from the bright contrast in the field ion image and single atom catching experiments in the atom probe are required [5]. Recent experiments in the local electrode atom probe have also demonstrated that the regions of the surface close to the center of high index planes should be avoided for this case as the solute atoms can be preferentially collected there during field evaporation giving the apparent appearance of a dislocation where none exists. In the other cases, the segregation will not be visible in the field ion image. These studies have been reviewed recently and so will not be discussed in detail [5–7]. Due to these limitations, atom probe tomography has superseded field ion microscopy for these types of analyses.

It should also be noted that the mechanical stress imposed on the specimen by the applied electric field needed to produce the field ion image seriously influences the configuration of the dislocation [8]. A consequence of this stress is that glissile dislocations will invariably slide out of the apex region of the specimen when the electric field is applied. Fortunately, solute segregation to or precipitation along the dislocations generally pins them sufficiently so that they can be characterized by atom probe tomography.

Atom probe tomography

Dislocations may also be observed in three-dimensional atom probe (3DAP) atom maps by enhanced levels of solute along linear features, as shown for a neutron irradiated Fe-1.6% Ni-0.025 at. % P model alloy in Fig. 1. In this atom map, each sphere represents a single phosphorus atom. For clarity, all the other elements are not shown. The dislocations are delineated by the enhanced local concentrations of phosphorus atoms. Until the introductions of the local electrode atom probe and more recently the wide-angle tomographic atom probe, the characterizations of dislocations have not been routinely performed in the atom probe due to their low densities in most materials and the limited volume of analysis. However, several examples of solute segregation to dislocations have been reported with the older variants of three-dimensional atom probe particularly in neutron irradiated pressure vessel steels and other alloys [9–16]. These studies have most often resulted from random
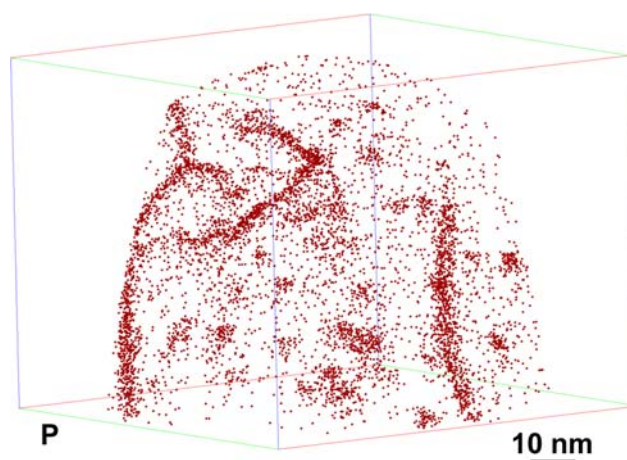

Fig. 1 Dislocations in an Fe-Ni-P model alloy that was neutron irradiated to a fluence of 1.8×10^{23} nm^{-2} ($E > 1$ MeV) at a temperature of 288 °C. Phosphorus segregation to the dislocations and some ~2-nm-diameter phosphorus clusters are evident. Material and irradiation courtesy of Prof. G. R. Odette, UCSB

encounter of a dislocation in the volume of analysis. One exception to this generality was a study of boron segregation to dislocations in single crystal boron-doped FeAl [10]. The advantage of the use of single crystals for this type of study is that the atom probe specimen can be prepared such that a known major crystallographic plane is normal to the major axis of the specimen so that these planes are then fully resolved in the atom maps and enables discontinuities such as major half planes, i.e., edge dislocations, and screw dislocations to be detected.

Preselection of suitable specimens may be made with the transmission electron microscope (TEM). The characterization of the electron transparent apex region of the needle-shaped specimen enables specimens containing dislocations to be selected. Due to the rapid rate of data analysis, direct characterization in the local electrode atom probe is more time efficient and avoids the additional manipulation of the specimen and hydrocarbon contamination. However, TEM characterization enables specimens containing dislocations in unreachable regions further along the shank of the needle to be additionally processed with the use of pulsed electropolishing or FIB-based techniques to remove small amounts of materials from the apex [9, 17]. Although the needle-shaped geometry is not ideal for the TEM due to the compound thickness variations, TEM characterization can also provide important crystallographic data on the character of the dislocation. TEM characterization cannot be performed after the atom probe analysis due to the destructive nature of the technique.

Examples of the type of information that may be gathered from dislocations is illustrated with a dataset from a beltline weld from the Midland reactor that was neutron irradiated to a fluence of 3.4×10^{23} m^{-2}, ($E > 1$ MeV). The atom map shown in Fig. 2 was obtained from a volume containing in excess of 20 million atoms. Examination of the volume reveals both a high number density of ultrafine copper-enriched precipitates together with several dislocations exhibiting phosphorus segregation. The copper-enriched precipitates result from the supersaturation of copper in the matrix of this steel and an irradiation enhanced precipitation rate. A comparison of the mechanical properties of the unirradiated and neutron irradiated conditions indicates a significant shift in the ductile-to-brittle transition temperature of ΔT_{41J} of 108 °C.

A discussion of the mechanical properties of this weld will be reported in detail elsewhere [18]. These copper-enriched precipitates are not evident in TEM micrographs due to a lack of contrast mechanisms in the Fe–Cu system. Atom probe tomography has demonstrated that these ultrafine copper-enriched precipitates are not present before neutron irradiation. However, some larger copper-rich precipitates are present after the stress relief treatment which decreases the excess copper in the matrix. Due to the relatively large extent of this volume ($63 \times 60 \times 228$ nm^3) and the small reproduced size, some of the detailed information is not apparent in this representation. Therefore, smaller selected volumes of this data are shown at higher magnification in Figs. 3 and 4. A dislocation network is shown in Fig. 3. Similar dislocation networks exhibiting carbon segregation i.e. Cottrell atmospheres, have been observed in a medium carbon steel [19]. The dislocation arrowed in Fig 2 is shown at higher resolution in Fig 4. This dislocation will be used to illustrate the quantification of size and compositions below. It is immediately apparent from these selected volumes that in addition to the phosphorus segregation to the dislocation, there is also preferential precipitation of the copper-enriched precipitates along the dislocation. The average interparticle distance along the dislocations was estimated to be 11 ± 3 nm. This distance is significantly smaller than that of the precipitates in the
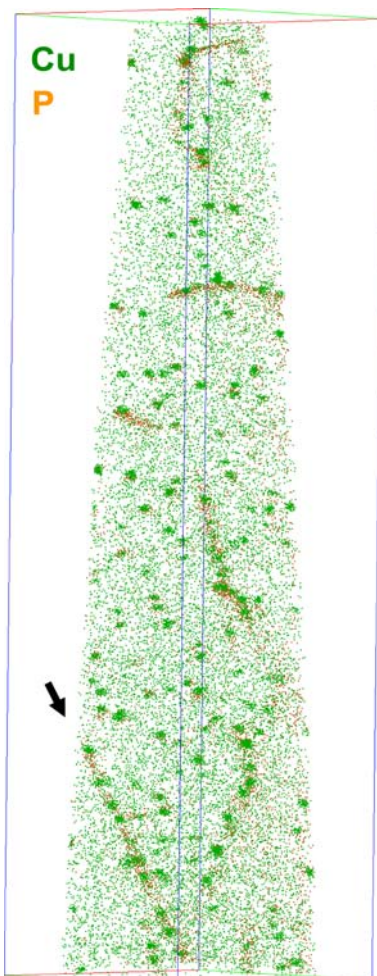

Fig. 2 Copper and phosphorus atom map of the beltline weld in the Midland reactor that was irradiated to a fluence of 3.4×10^{23} nm^{-2} ($E > 1$ MeV). Phosphorus segregation to the dislocations and a high number density of ~2-nm-diameter copper-enriched precipitates are evident. Arrowed dislocation is shown at higher resolution in Fig. 4
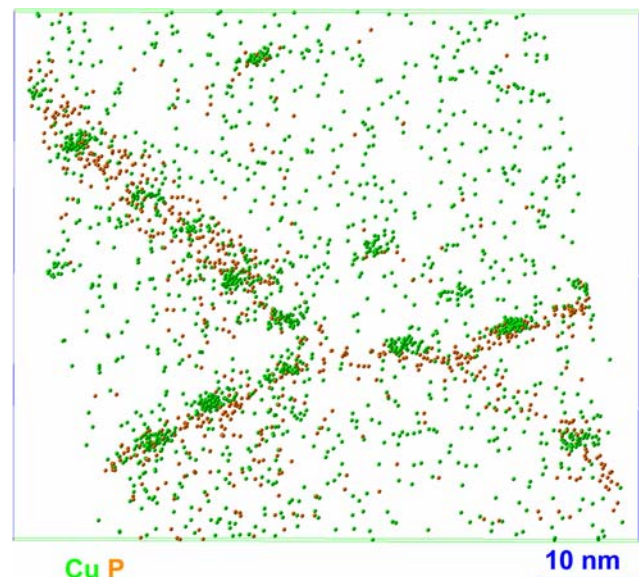

Fig. 3 High resolution copper and phosphorus atom map of a dislocation network in the beltline weld in the Midland reactor that was irradiated to a fluence of 3.4×10^{23} nm^{-2} ($E > 1$ MeV). Phosphorus segregation to the dislocations and preferential precipitation of ~2-nm-diameter copper-enriched precipitates on the dislocations are evident

Fig. 4 High resolution copper and phosphorus atom map and 2D phosphorus concentration map of a selected volume surrounding the dislocation arrowed in Fig 2. Phosphorus segregation to the dislocations and preferential precipitation of ~2-nm-diameter copper-enriched precipitates on the dislocation are evident
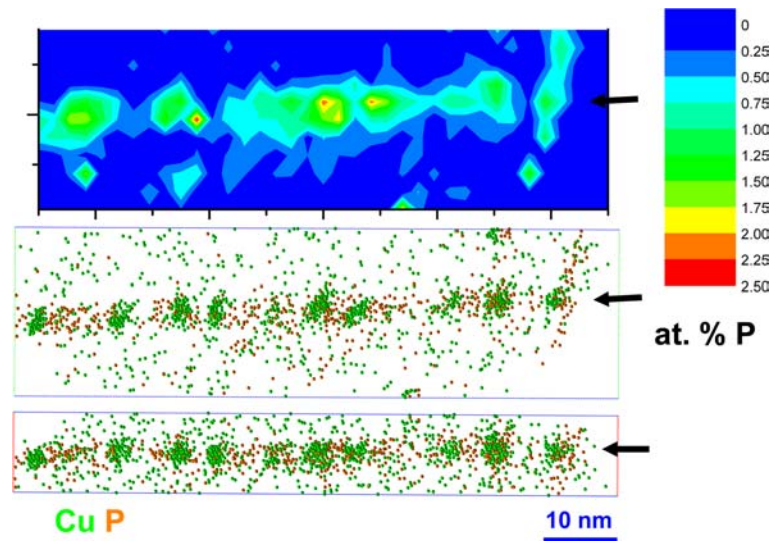
matrix and indicates preferential nucleation on the dislocations.

The size and composition of the copper-enriched precipitates and the level and extent of the phosphorus segregation can be estimated from the atom probe data. The standard methods [9] such as manually defining selected volumes that encompass the feature of interest or creating concentration profiles along small cross section cylinders intersecting the feature of interest are inefficient and not effective at this nano-meter size range. Two computational methods have been found to be effective for these situations. The maximum separation or friends-of-friends (FOF) method is based on the principle that the solute atoms in a solute-enriched region (i.e., the copper-enriched precipitate and the region of enriched phosphorus in the vicinity of the core of the dislocation) are closer together than those atoms in the more dilute matrix [20, 21]. Therefore, these regions may be located in the three-dimensional data by searching for those atoms that are within a certain distance, d_{max}, of another solute atom of the same type or group of types. The magnitude of the separation distance depends on the solute concentrations in the precipitates and the matrix and is generally of the order of a few nearest neighbor distances (i.e., ~0.3 to ~0.7 nm). This distance param-eter is defined from simulations or atom probe analysis of random solid solutions. Once these atoms have been found, the center of mass and the radius of gyration can be calculated from standard formulae [9]. The average radius of gyration of the copper-enriched precipitates in the weld was estimated with a d_{max} parameter of 0.6 nm to be 0.87 ± 0.17 nm. This yields an average Guinier radius of 1.1 ± 0.2 nm. Both these estimates are slightly underestimated due to the difference in

magnification between the precipitates and the sur-rounding matrix due to their different evaporation fields. This underestimation can be corrected for as the local apparent atomic density can also be estimated from the atom probe data. In this example, no appre-ciable difference was observed in the sizes or the compositions of the precipitates in the matrix and on the dislocations. This maximum separation method may also be used to remove the matrix solute in the atom maps thereby improving the visibility of the segregation [9].

This method may be adapted to features of any geometry. In the case of a dislocation, a volume is selected around each dislocation so that the line of the dislocation runs along the major axis of the volume. This adaptation enables the 2 radii of gyration in the lateral directions normal to the line of the dislocation to be estimated. The average radius of gyration of the phosphorus segregation to the dislocation shown in Fig. 4 was estimated to be 0.6 ± 0.2 nm.

The tracer method can be used to estimate the level of segregation at the dislocation or interfaces. This method also involves the creation of a selected volume containing the feature(s) of interest. In the dislocation example shown in Fig. 4, the cross section of the volume was 10 nm × 21 nm. A fine 3D grid is then superimposed on this volume and the composition of all the cells are estimated from the number of the different types of atoms within each cell. The maxi-mum concentration of the element(s) of interest along each column in the grid is determined for all the columns in each of the three orthogonal directions. This process generates a 2-dimensional representation of the concentrations of all the elements in each of these orthogonal directions. The phosphorus concentration

map for one of those directions is shown in Fig 4. In this example, the phosphorus enrichment was estimated to be ~1 at. % P with local maxima of up to ~2.5 at. % P. This represents phosphorus enrichments of ~30–80 times that of the alloy composition. Multiple element segregation to dislocations can also be quantified as shown for a dislocation in a mechanically alloyed, oxide dispersion strengthened (MA/ODS) ferritic alloy [15].

The partitioning of the other alloying elements to the copper-enriched precipitates and interfacial segregation may also be investigated from these data. High-resolution atom maps of a typical individual precipitate are shown in Fig. 5. These maps reveal that manganese, nickel, silicon and phosphorus partition to the precipitate. In addition, the extents of the manganese, nickel and silicon atoms are larger than that of copper atoms. The composition of these ~2-nm-diameter precipitates may be estimated with the envelope method [9]. In this method, a three-dimensional grid of volume elements is superimposed on the 3D data. To retain the inherent spatial resolution of the APT technique, the grid spacing is generally chosen to be less than 0.2 nm. The volume elements that contain the selected (i.e., copper) atoms, as determined from the maximum separation method, are marked. Some cells with no selected atoms that are surrounded with marked cells are also included due to the small number of atoms in each cell. The solute concentrations of all the marked cells for each precipitate are then determined by counting the number of atoms of all elements in each volume element. The compositions of the core of these precipitates, as estimated from the envelope method based on the maximum separation of copper atoms and a grid size of 0.1 nm, was estimated to be Fe–83.4 ± 5.1% Cu, 1.2 ± 0.9% Ni, 0.8 ± 0.6% Mn, 0.7 ± 0.6 % Si.

If, as in this case, the features are spherical, radial concentration profiles from the center of mass into the surrounding matrix may also be constructed to investigate interfacial segregation of the different solutes. For example, an averaged radial concentration profile from 30 of these copper-enriched precipitates that extends from the center of mass into the matrix for copper, nickel, manganese and silicon is shown in Fig. 6. The partitioning of nickel, manganese and silicon to both the core of the precipitate and enrichments at the precipitate-matrix interface are evident. A slight tail of these solutes into the matrix is also evident.

It is reasonable to conclude that the shift in the ductile-to-brittle transformation temperature of this beltline weld from the Midland reactor arises from the interaction of dislocations with the high number density of these ~2-nm-diameter copper-, manganese-,
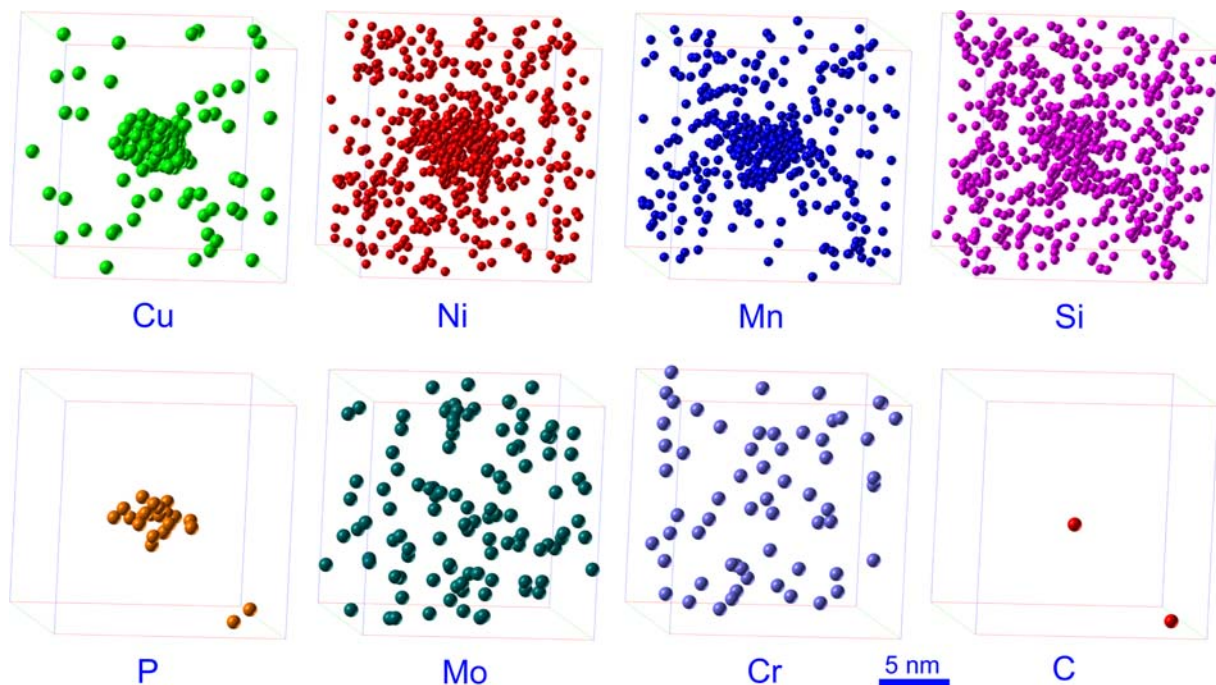

Fig. 5 High resolution atom maps of the alloying elements for an individual precipitate in the beltline weld in the Midland reactor that was irradiated to a fluence of 3.4×10^{23} nm^{-2} ($E > 1$ MeV). The extents of the manganese, nickel and silicon atoms are larger than that of copper atoms
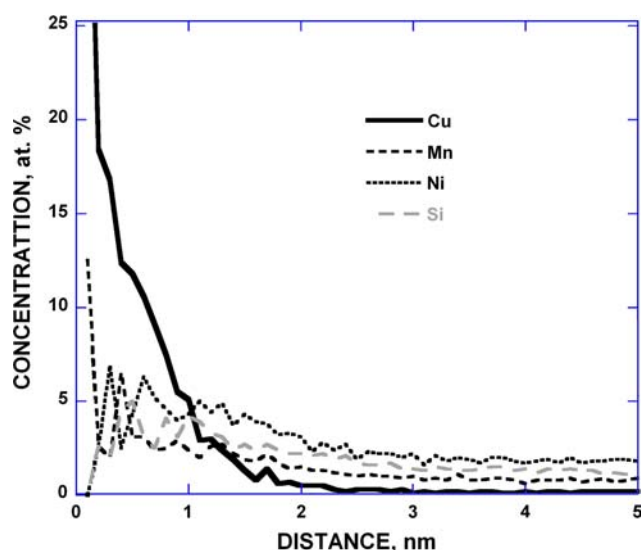
Fig. 6 An average radial concentration profile from the centre of mass of the copper-enriched precipitates out into the ferrite matrix for the weld from the Midland reactor that was irradiated to a fluence of 3.4×10^{23} nm^{-2} ($E > 1$MeV)

nickel- and silicon-enriched precipitates. The solute enrichments at the precipitate-matrix interface and the phosphorus segregation to the dislocation also contribute to the embrittlement process as they will further impede the motion of the dislocations.

Summary

Atom probe tomography enables the extent and level of solute segregation at dislocations to be estimated. The wide field of view instruments such as the local electrode atom probe are particularly suitable for this application. In addition, fine scale precipitation along the dislocation may be characterized. Examples were presented of phosphorus segregation to dislocations in a neutron irradiated Fe–Ni–P model alloy and the neutron irradiated beltline weld from the Midland reactor. The technique is best applied to materials with high dislocation densities due to the relatively limited volume of analysis. In lower dislocation density materials, the transmission electron microscope together with pulse polishing or FIB-based methods may be used to select and fabricate suitable specimens. The level of solute segregation at the interfaces of nanometer scale precipitates may also be estimated with this technique.

References

1. Bowkett KM, Smith DA (1970) Field Ion Microscopy. North Holland, New York, NY, pp. 104–141–145–149
2. Miller MK, Horton JA (1987) J de Phys 48-C6:379
3. Jayaram R, Miller MK (1995) Scripta Metall 33:19
4. Chang L, Barnard SJ, Smith GDW (1992) In: Krauss G, Repas PE (eds) Fundamentals of aging and tempering in Bainitic and Martensitic steel products, The Iron and Steel Society, Warrendale, PA, p 19
5. Miller MK, Cerezo A, Hetherington MG, Smith GDW (1996) Atom probe field ion microscopy. Oxford University Press, Oxford, UK
6. Miller MK (2004) TMS Lett 1:19
7. Miller MK (2006) Microsc Res Tech 69:359
8. Smith DA, Birdseye PJ, Goringe MJ (1973) Phil Mag 27:1175
9. Miller MK (2000) Atom probe tomography. Kluwer Academic/Plenum Press, New York, NY
10. Blavette D, Cadel E, Fraczkiewicz A, Menand A (1999) Science 286:2317
11. Wilde J, Cerezo A, Smith GDW (2000) Scripta Mater 43:39
12. Miller MK, Russell KF, Kocik J, Keilova E (2000) J Nucl Mater 282:83
13. Miller MK, Pareige P (2000) In: Lucas GE, Snead LL, Kirk MA, Elliman RG (eds) Material Research Society Symposium R: Microstructural processes in irradiated materials, November 27–29, 2000, vol. 650, Material Research Society, Warrendale, PA, p R6.1.1
14. Miller MK, Russell KF, Kocik J, Keilova E (2001) Micron 32:749
15. Miller MK, Kenik EA, Russell KF, Heatherly L, Hoelzer DT, Maziasz PJ (2003) Mater Sci Eng A A353:140
16. Pareige P, Radiquet B, Suvorov A, Kozodaev M, Krasikov E, Zabusov O, Massoud JP (2004) Surf Interface Anal 36:581
17. Miller MK, Russell KF, Thompson GB (2005) Ultramicroscopy 102:287
18. Sokolov MA, Nanstad RK (2006) Proceedings of ASME Pressure Vessels and Piping Division Conference, July 23–27, 2006, Vancouver, BC, Canada, in press
19. Pereloma EV, Miller MK (2005) Microsc Microanal 11(suppl. 2):876
20. Hyde JM (1993) Computer modeling and analysis of microscale phase transformations, D. Phil Thesis, Oxford University, Oxford, UK
21. Hyde JM, English CA (2001) In: Lucas GE, Snead L, Kirk MA Jr, Elliman RG (eds) Proceedings of MRS 2000 Fall Meeting, Symposium R: Microstructural processes in irradiated materials, Boston, MA, November 27–30, 2000, vol. 650, Materials Research Society, Pittsburgh, PA, p R6.6.1